Presented at the International Symposium on Nuclear Spectroscopy and Nuclear Interactions, Osaka, Japan, March 21-24, 1984

CONF-8403112--6

# PHOTON DECAY OF GIANT RESONANCES

F. E. Bertrand, J. R. Beene, and M. L. Halbert†
Oak Ridge National Laboratory*
Oak Ridge, Tennessee 37831, U.S.A.

CONF-8403112--6

DE85 001101

NOTICE
PORTIONS OF THIS REPORT ARE ILLEGIBLE.
It has been reproduced from the best available copy to permit the broadest possible availability.

## ABSTRACT

Measurements have been made of the photon decay of the giant multipole resonances in $^{208}Pb$. The giant resonances were excited by inelastic scattering of 380 MeV $^{17}O$ projectile and the photons were detected in the ORNL Spin Spectrometer. The results show a quadrupole resonance ground state gamma branch of 20% while only $\lesssim 2\%$ of the GQR decay proceeds through the 2.6 MeV, $3^-$ state. Nearly one half of the GQR decay through a $3^-$ state at 4.974 MeV. Photon decay from the dipole and monopole resonances and high spin resonances ($4^+$,$6^+$) are also observed.

Over the past decade several new giant resonances have been observed and classified.[1] Most of the observation of these new resonances has been accomplished through the use of light mass hadronic probes (protons, alphas, etc.), utilizing either inelastic scattering or charge exchange reactions. Recently, some advantages to excitation of isoscalar giant resonances using inelastic scattering of medium energy heavy ions have been investigated.[2]

MASTER

Figure 1 shows an example of isoscalar giant resonances excited in several targets by inelastic scattering of 152-MeV alpha particles.[3] In each spectrum a broad peak is observed at an excitation energy that varies smoothly with target mass. This peak contains both the isoscalar giant quadrupole (GQR) and monopole (GMR) resonances, and, at least for the case of $^{208}Pb$, it has been shown[4] that some hexadecapole resonance strength (GHR) is also present. In inelastic excitation of the giant resonances the multipolarity of the resonance and the fraction of the energy weighted sum rule (EWSR) depleted in the observed peak are determined from a comparison of the measured and calculated angular distributions. Figure 2 shows such a

---

†Collaborators on the ORNL work reported here are: R.L. Auble, E.E. Gross, D.C. Hensley, D.J. Horen, R.L. Robinson, R.O. Sayer, D. Shapira, and T.P. Sjoreen.

*Operated by Martin Marietta Energy Systems, Inc. under contract DE-AC05-84OR21400 with the U.S. Department of Energy.

DISTRIBUTION OF THIS DOCUMENT IS UNLIMITED

By acceptance of this article, the publisher or recipient acknowledges the U.S. Government's right to retain a nonexclusive, royalty-free license in and to any copyright

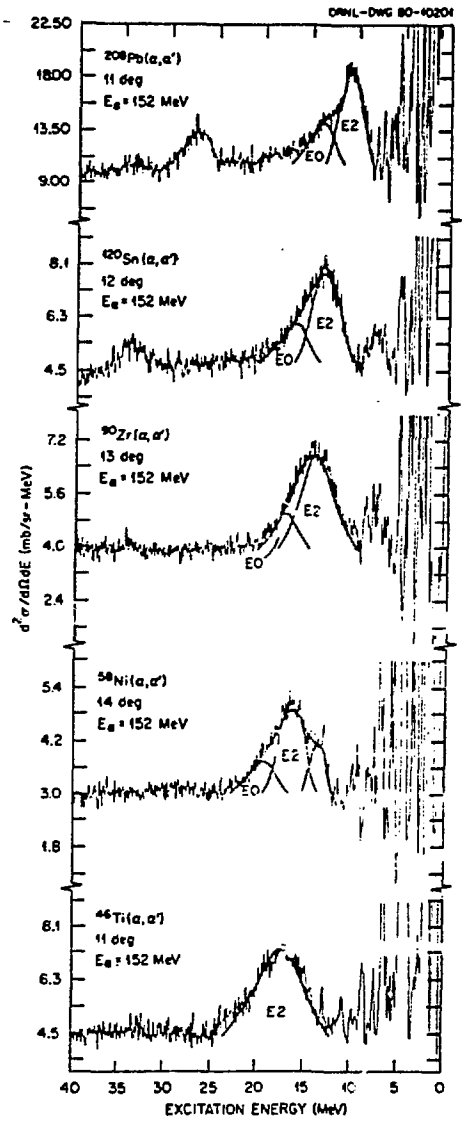


Fig. 1. Spectra from inelastic scattering of 152-MeV alpha-particles on $^{208}Pb$, $^{120}Sn$, $^{90}Zr$, $^{58}Ni$ and $^{46}Ti$. The giant resonance structure located near the excitation energy $63 \times A^{-1/3}$ MeV has been decomposed into contributions from the giant quadrupole and giant monopole resonances. The peak located at higher excitation energy in the $^{208}Pb$ and $^{120}Sn$ spectra is due to hydrogen contamination of the target.

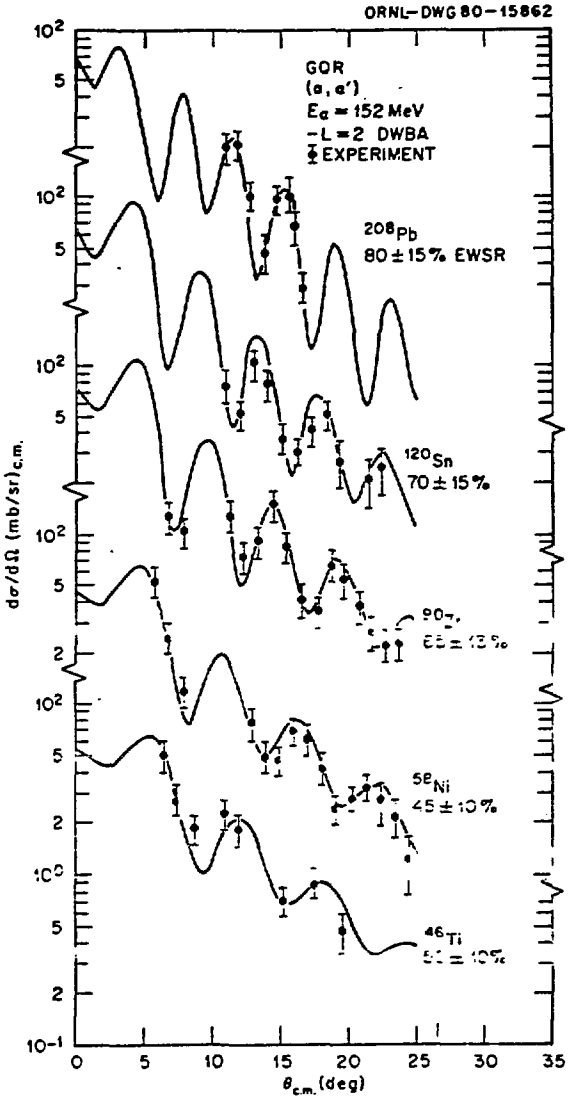


Fig. 2. Angular distribution of the E2 portion of the spectra from fig. 1. The data are compared to an L=2 DWBA calculation normalized to the indicated EWSR depletions (ref. 7).

comparison for the "E2" part of the spectra shown in figure 1. The data are shown compared to Distorted Wave Born Approximation (DWBA) calculations for L=2 excitations in each target. By normalizing the calculations to the data a deformation parameter, $\beta_2$, is extracted from which the percentage depletion of the appropriate EWSR strength can be deduced.[1] From measurements such as these the location, width and strength of several isoscalar giant resonances have been determined in a large number of stable nuclei.

However, the procedure described above for observation of isoscalar resonances is not without considerable uncertainty. There is, of course, the uncertainty of extraction of the GR peak cross section from the very large underlying nuclear continuum. The DWBA calculated cross sections are dependent upon the optical model parameters used for the calculation. Furthermore, unlike the case for electromagnetic transitions, the extraction of a transition rate from inelastic scattering is model dependent and often does not agree with results from Coulomb excitation or electron scattering. Figure 3 points out another difficulty. The figure schematically represents single-particle transitions between shell-model states of a hypothetical nucleus. Collective transitions result from coherent superpositions of many such single-particle transitions. Major shells are denoted as N, N+1, etc. and are separated by $\sim 1\hbar\omega$ or $\sim 41\ A^{-1/3}$ MeV. Giant resonances may be considered to result from transitions of nucleons from one major shell to another, under the influence of an interaction that orders these transitions into a coherent motion. The interaction for inelastic scattering can excite a nucleon by at most $L\hbar\omega$, or, to state it differently, the nucleon can be promoted by at most L major shells. The number of shells is either odd or even according to the parity.

Thus, the isovector giant dipole resonance (GDR) is built up of E1 transitions spanning $1\hbar\omega$. The GDR might then be expected to be located at an excitation energy of $\sim 41\ A^{-1/3}$ MeV; however, it is located at $\sim 77\ A^{-1/3}$ MeV. This difference arises from the fact that

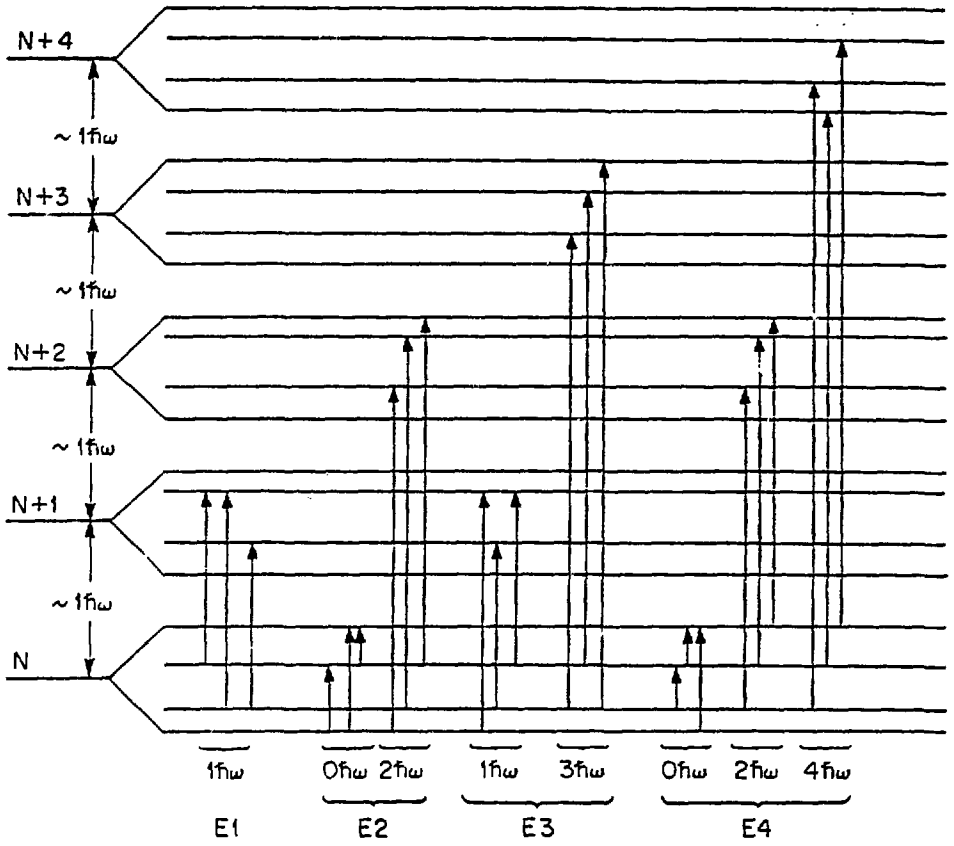


Fig. 3. Schematic representation of electric multipole transitions between shell-model states of a hypothetical nucleus. Major shells are denoted as N, N+1, N+2, etc. and lie ~ 1ħω or ~ 41 x $A^{-1/3}$ MeV apart.

the spin and isospin dependence of the nucleon-nucleon interaction ensures that the S=T=0 collective states move down in energy, and that S=1 or T=1 states move up from the expected energy.

For E2 excitations two different classes of transitions are allowed. The first of these, with lowest energy, is comprised of transitions within a major shell, the so-called 0ħω transitions. A second set is comprised of transitions between shells N and N+2, the 2ħω transitions. These transitions would be pushed up or down in energy from 2ħω for isovector or isoscalar modes respectively. While

the $0\hbar\omega$, E2, excitations are identified with the familiar low-lying $2^+$ levels, the $2\hbar\omega$ class carry most of the EWSR and are associated with the GQR. By similar arguments E3 excitations of $1\hbar\omega$ and $3\hbar\omega$, E4 excitations of $0\hbar\omega$, $2\hbar\omega$ and $4\hbar\omega$, E5 excitations of $1\hbar\omega$, $3\hbar\omega$ and $5\hbar\omega$ and E6 excitations of $0\hbar\omega$, $2\hbar\omega$, $4\hbar\omega$ and $6\hbar\omega$ are expected.

Clearly, this situation leads to the potential for giant resonance states of different multipolarity to overlap in the nuclear continuum. The possible confusion is further heightened when the spectra of giant resonance states are considered with their considerable damping widths and estimates of their strengths.

While some selectivity in GR excitation is obtained in inelastic scattering by selection of the incident particle (e.g., the T=0 alpha particle only excites the isovector giant dipole resonance via Coulomb excitation) in general inelastic scattering is not selective among the various multipoles. It is of considerable importance to find a method to study the complicated GR structure that would provide multipole selectivity and would at the same time provide a model independent measure of the transition strength in the resonance. We believe a measurement of the photon decay of the giant resonances can provide such information and for the past year we have carried out a program of $\gamma$-decay measurements.

The measurements were carried out by exciting the giant resonances using 380 MeV $^{17}O$ inelastic scattering and detecting the $\gamma$-decay (in coincidence with the inelastically scattered $^{17}O$) in a $4\pi$, $\gamma$-ray spectrometer. The use of $\sim$ 25 MeV/amu $^{17}O$ inelastic scattering provides very large cross sections and excellent peak-to-continuum ratios for the GQR. This is pointed out in figure 4 where we show a comparison between the giant resonance structure observed in $^{208}Pb$ as excited by 400-MeV $^{16}O$ ions and 152-MeV alpha particles. The two spectra are normalized at 22 MeV of excitation energy. The solid line drawn under both spectra indicates only an approximate "background" level that may be used as an aid to compare the two spectra. The solid curves in each spectrum are the shapes of

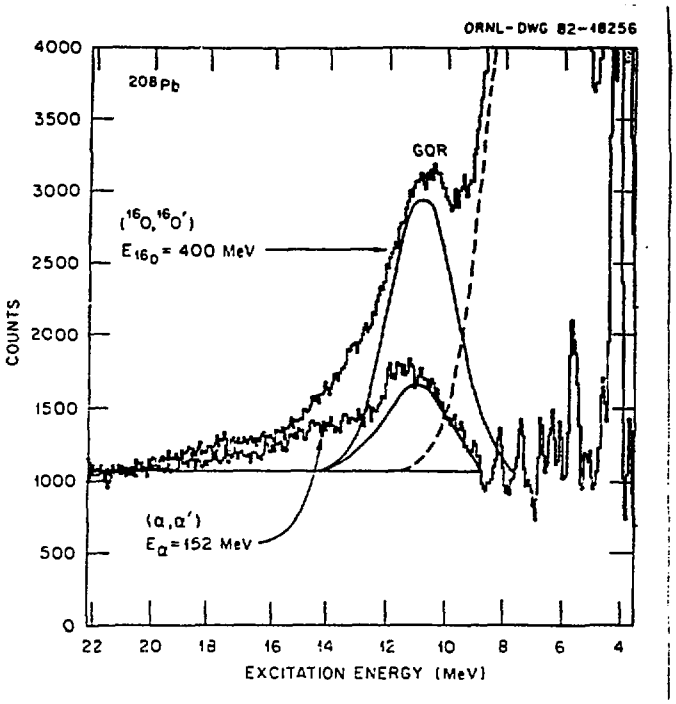


Fig. 4. Comparison of $^{208}Pb$ giant resonance spectra as obtained from the $(^{16}O, ^{16}O')$ reaction at 400 MeV and the $(\alpha, \alpha')$ reaction at 152 MeV. The spectra are normalized at 22 MeV.

the GQR peak. The heavy ion spectrum contains a very large peak from excitation of states in the $^{16}O$ projectile. This effect is, of course, not present in the alpha particle scattering so that much more structure is seen below the giant resonance peak. The most obvious difference in the two spectra is the very much larger peak-to-continuum ratio in the case of the heavy-ion scattering, over twice that observed with alpha particles. The cross section for 400 MeV $^{16}O$ on $^{208}Pb$ reaches a maximum value of ~ 60 mb/sr at the grazing angle (~ 11.5 degrees).

While the peak-to-continuum ratio for giant resonance spectra from heavy-ion inelastic scattering shows considerable improvement over spectra obtained with alpha particles or protons, heavy-ion excitation has a serious disadvantage in the angular distributions. Figure 5 shows calculated angular distributions for the inelastic excitation of L=2, 3 and 4 states at 10.9 MeV by 400 MeV $^{16}O$ ions. Except for some small differences at very small angles, the angular distributions all look alike. This fact makes heavy-ion angular distributions nearly

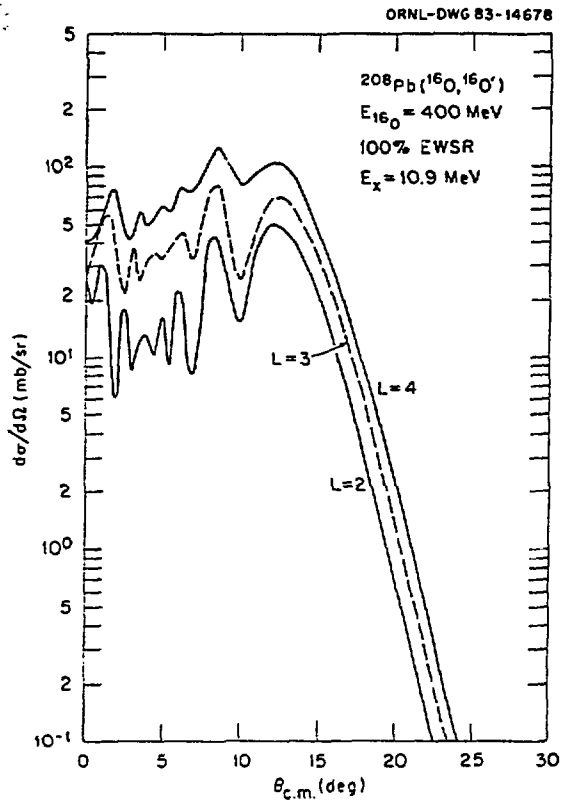


**Fig. 5.** Calculated angular distribution for L=2,3, and 4 states in $^{208}Pb$ excited by inelastic scattering of 400 MeV $^{16}O$ ions. The calculations are normalized to 100% of the EWSR for each multipolarity.

useless for multipolarity identification, at least in this general energy range.

Figure 6 shows some of the $^{208}Pb$ levels which are relevant to the present decay measurements. The giant resonances are shown as broad states lying between ~ 9 and 16 MeV. In this study we deal with the 10.6 MeV, 2.4 MeV wide GQR, the 13.9 MeV, 3.6 MeV wide GMR, and the 13.9 MeV, 4.0 MeV wide GDR. These giant resonances lie well above the particle thresholds. However, the large Coulomb barrier ensures that the decay of the resonances is overwhelmingly dominated by neutron decay. Indeed, the photon decay branch of the GQR can be estimated to be (for 100% of the EWSR and a 2.4 MeV wide state) only ~ $10^{-4}$ of the total decay of the state. The neutron decays will, of course, populate rather low-energy states in $^{207}Pb$.

There are primarily two experimental capabilities available at ORNL that contributed to our successful γ-decay measurements. The first, discussed above, is the use of ~ 25 MeV/amu heavy ions that

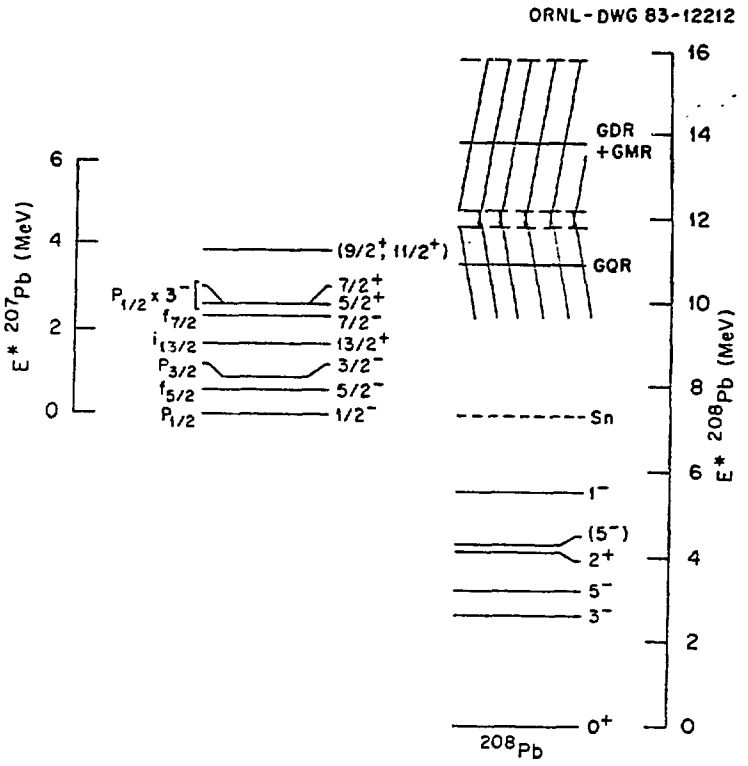


Fig. 6. Selected levels in $^{208}Pb$ and $^{207}Pb$. The configuration labels on the $^{207}Pb$ states refer to neutron hole states.

excite the giant resonances with large cross sections and yield large resonance peak-to-continuum ratios. We chose $^{17}O$ because the particle thresholds are very low and thus the projectile excitation cross section near the GR region in $^{208}Pb$ in coincidence with outgoing $^{17}O$ is negligible. The second, and certainly most important, feature is the existence at ORNL of the Spin Spectrometer,[5] a crystal-ball device, which is a $4\pi$, segmented NaI gamma ray spectrometer consisting of 72 NaI detectors (see figure 7). Each detector is 17.8 cm thick and ~ 7.6 cm in diameter at the front and 15.2 cm diameter at the back. In the present experiment (shown in figure 7), the NaI elements at 0° and 180° (relative to the beam direction) were removed for the beam entrance and exit pipes. Figure 7 shows one half of the

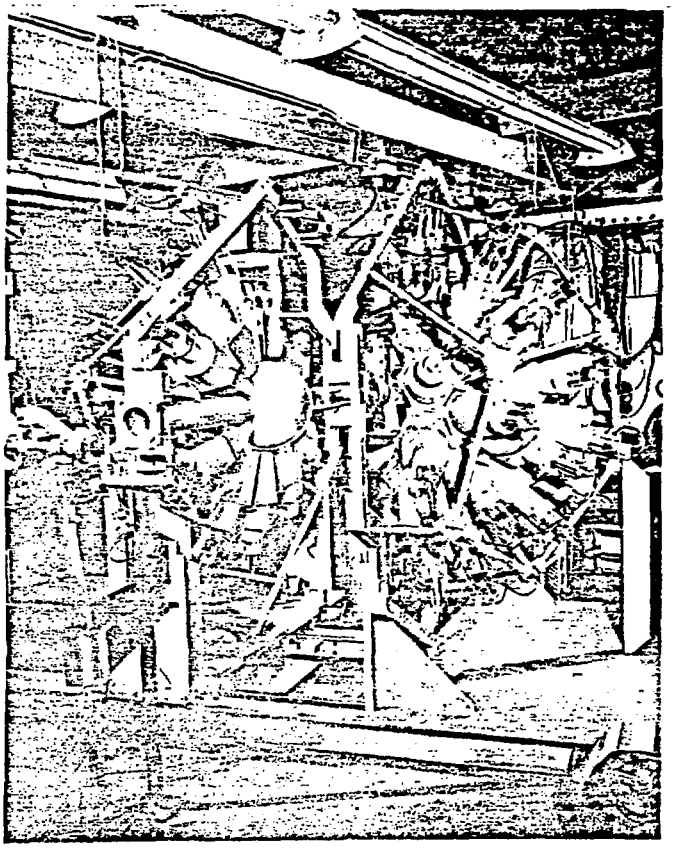

Fig. 7. ORNL Spin Spectrometer. The spectrometer is shown with one half pulled back to expose the spherical scattering chamber.

spectrometer pulled back to expose the 16.5 cm radius scattering chamber in the center. The Spin Spectrometer with its nearly $4\pi$ geometry provides high efficiency detection[5] for both gamma radiation and neutrons. Neutrons and gamma rays were distinguished by time of flight. The flight path is too short to permit resolution of neutron decay to individual levels in $^{207}$Pb. However, the residual excitation energy in $^{207}$Pb following neutron emission is accurately determined from the total gamma-ray energy in the Spin Spectrometer.

Charged reaction products were detected in six Si surface barrier detector telescopes each consisting of a 500 μm thick ΔE and a 1500 μm thick E detector. As is shown in figure 8 these detector telescopes provided excellent mass separation. The telescope mount is shown in figure 9. The pipe connections are for cooling liquid. Each

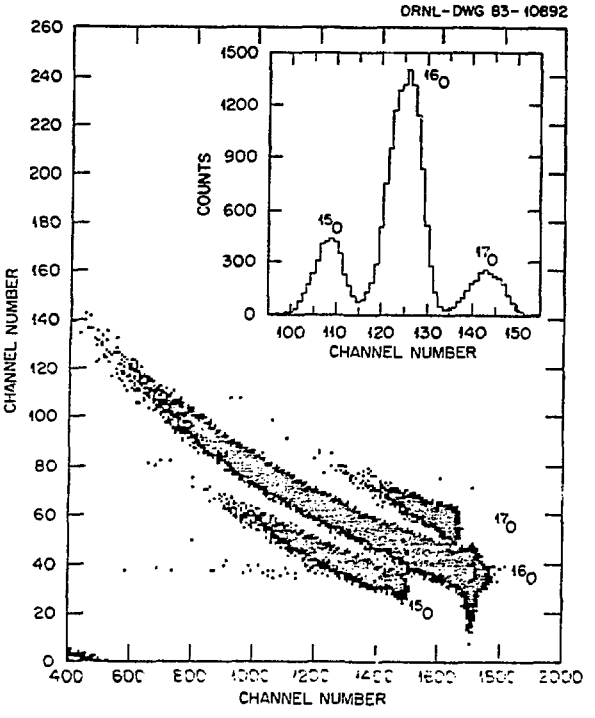


Fig. 8. ΔE-E spectra for oxygen isotopes from reaction $^{208}Pb(^{16}O,^{16}O')$ at 400 MeV (ΔE-ordinate, E-abscissa).

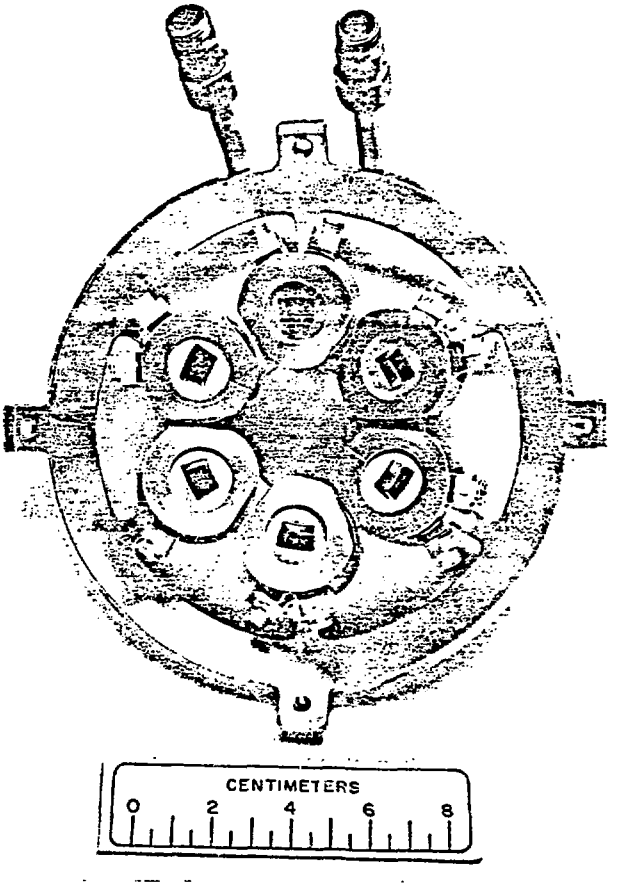


Fig. 9. Mount for the charged particle telescopes. The detectors are in place behind the trapezoidal collimators.

telescope was covered with a trapezoidal collimator having an opening angle of $\Delta\theta = 3°$ and $\Delta\phi = 9°$, yielding a total solid angle for the array of 22.6 msr. Figure 10 shows the charged-particle detector array mounted inside the Spin Spectrometer scattering chamber. A target is seen in the chamber center and NaI elements surround the chamber.

The E and $\Delta E$ signals from each telescope were gain matched and summed for total energy which along with the $\Delta E$ signal, NaI pulse heights, the time between the particle telescope trigger and each NaI detector pulse, and the time of the telescope trigger relative to the cyclotron r.f., were digitized for each event.

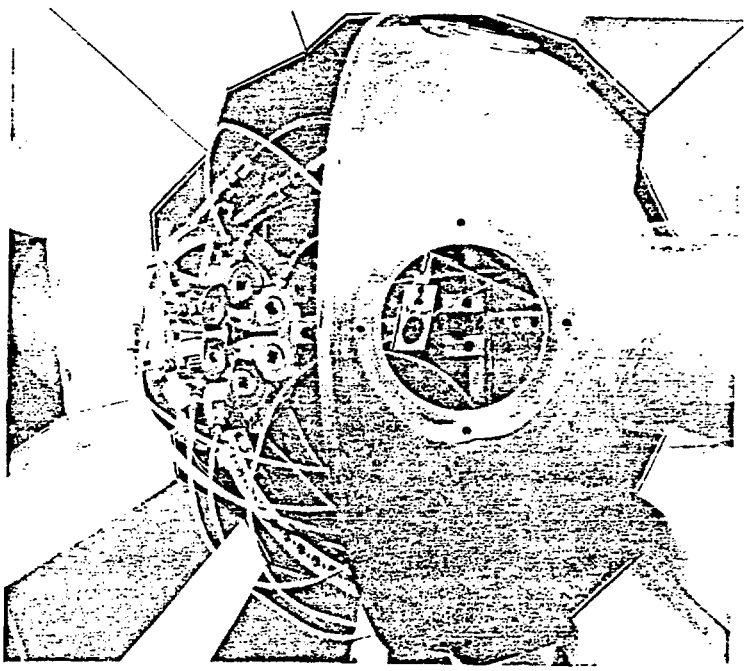

Fig. 10. An internal view of the scattering chamber with the charged particle telescopes mounted. The beam enters through the pipe at the right, strikes the target seen through the window, and then exits through the hole in the center of the detector mount. The exit hemisphere of the scattering chamber was removed for this photograph.

We have calibrated the NaI detectors for high energy $\gamma$ rays using the $^{12}C(p,p')^{12}C$ reaction with 24-MeV protons. This reaction, in which we detected the inelastically scattered protons in coincidence with the decay $\gamma$ rays, provides energy and efficiency calibration for, among others, 4.43-, 12.71- and 15.11-MeV gamma rays. Additional calibration for lower energy gamma rays was performed using radioactive sources.

Events which involved pure $\gamma$ decays were isolated by specifying two criteria. a) No neutron pulse was seen by the spectrometer, and b) the total energy carried away by gamma radiation accounted, within the resolution of the detectors involved, for the total excitation energy of $^{208}Pb$ in the event, as determined by the energy of the inelastically scattered $^{17}O$.

This isolation of gamma decay events is illustrated in Figure 11 which shows a two-parameter histogram of events in which NaI pulses were detected in coincidence with a charged particle identified as $^{17}O$ in one of the telescopes. The abscissa is the excitation energy in the initial $^{208}Pb$ nucleus derived from the energy of the $^{17}O$. The ordinate is the sum of the gamma ray energies detected in the spectrometer. These should be events in which no neutron pulse was detected, but since virtually all the GR decay is via neutrons [above $E^*(^{208}Pb) \sim 8$ MeV], and since the neutron detection efficiency is less than 100%, the requirement of the absence of a neutron pulse still leaves a substantial background of n-decay events. However, these background events are well separated from pure $\gamma$-decay events because of the neutron separation energy, $S_n$. The pure gamma-decay events should be found in the region outlined on Figure 11, for which the sum $E_\gamma$ is approximately equal to $E^*(^{208}Pb)$. In order to avoid confusion from the detection of high energy particles from the sequential decay of $^{18}O$ and $^{18}F$ back to $^{17}O$ following transfer reactions, an event was considered for further analysis only if the largest pulse height occurred in a NaI element at $\theta_{lab} > 66°$. Figure 11a shows all $\gamma$ rays that fulfill the above requirements. The yield of these events is

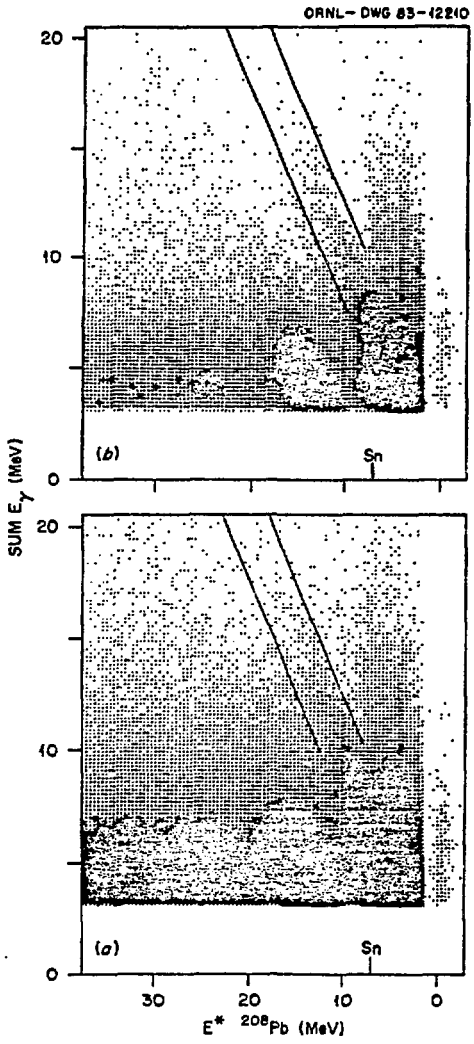


Fig. 11. (a) Is a plot of all events in which no delayed pulse (neutron) was observed. The solid lines indicate the boundaries of the region for which sum $E_\gamma \sim E^*$ $^{208}$Pb (they should extend to sum $E_\gamma = 0$). In (b) the additional constraint $V > 0.95$ has been applied.

found to fall off approximately exponentially above $S_n$. The total gamma branching ratio at 11 MeV is $\sim 2 \times 10^{-3}$.

It is important to select those gamma events which decay directly to the ground state. Unfortunately the number (k) of gamma detectors which are triggered in an event is not useful for this selection. The calibration experiments show that a single 15.1 MeV gamma ray triggers, on the average, about three detectors and has a significant probability to trigger as many as five. Therefore, we have used the parameter

$$V = \left| \sum_{i=1}^{k} \vec{h}_i \right| / \sum_{i=1}^{k} \left| \vec{h}_i \right|$$

to sort out ground state gamma decays. The $h_i$ are the individual gamma ray pulse heights recorded in an event. These pulse heights can be assigned a direction as well as a magnitude by noting the position in the Spin Spectrometer array of the detector which produced them; hence, a "vector pulse height," $\vec{h}$, (or apparent photon momentum vector) is obtained for each triggered detector. V is the ratio of the magnitude of the vector sum of pulse heights to the scaler sum. The ratio is represented schematically on figure 12 for two extreme types of events. For an event resulting from a single gamma ray this quantity should be near one since only adjacent detectors are triggered. For a cascade decay involving multiple gamma rays V should approach zero as the number of gamma-ray increases. Figure 11b is the same plot as 11a, subject to the additional requirement that $V > 0.95$. It is clear that the rarity of the ground state, GR $\gamma$-branch among the large "background" of high-multiplicity cascade $\gamma$-ray events requires a device having many $\gamma$ detectors and $4\pi$ geometry like the Spin Spectrometer.

Figure 13 shows the sum gamma-ray spectra obtained from the two-dimensional plots such as figure 11. The results shown in figure 13 are from those events located between the masks (diagonal lines) on figure 11. The solid curve on figure 13 is the $\gamma$-ray spectrum for all values of V, i.e. all gammas, and corresponds to the data on figure 11a. The dashed curve corresponds to $\gamma$-events for which $V > 0.98$ (figure 11b) and consists only of gamma rays from ground state transitions. The peak at 2.61 MeV from the $3^-$ state decay has the same number of counts in both spectra. This is of course expected since the state decays 100% to the ground state. On the other hand, in the region above ~ 10 MeV the total $\gamma$-branch exceeds the ground state $\gamma$-branch by factors of 5-10.

Figure 14 shows the ratio of the solid and dashed gamma-ray spectra in figure 13, which is equal to the ground state gamma ray branching ratio, $\Gamma\gamma_o/\Gamma\gamma_{Total}$. Figure 14 shows the regions of excitation in $^{208}Pb$ which have strong electromagnetic matrix elements to the

$$V = \frac{|\Sigma h_i|}{\Sigma |h_i|}$$

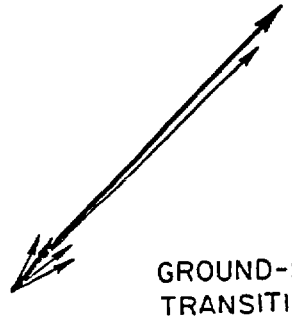

GROUND-STATE
TRANSITION
V~1

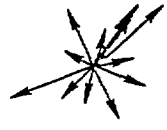

CASCADE
V~0

Fig. 12. Schematic representation of method for selecting ground-state γ-ray transitions. The heavy arrow is the vector sum of the transitions in typical single events for (a) ground-state transition or (b) cascade decay to ground state. The magnitude of the parameter V distinguishes between the two.

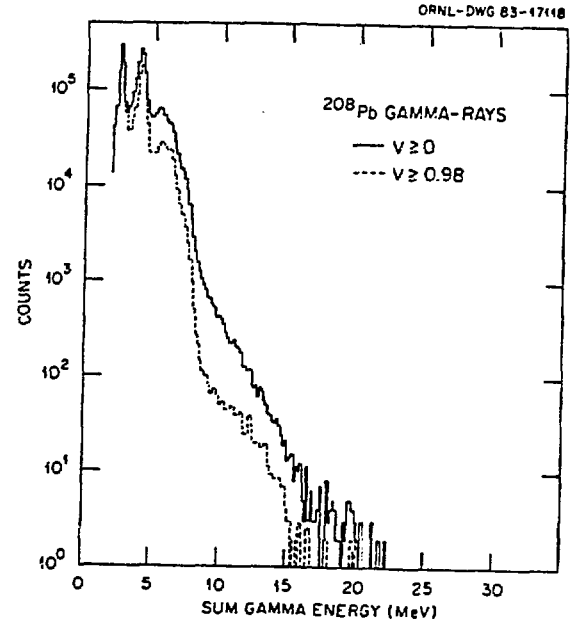


Fig. 13. Gamma-ray spectra from $^{208}Pb$ for V > 0 (all gamma rays) and V > 0.98 (only ground state gamma rays.

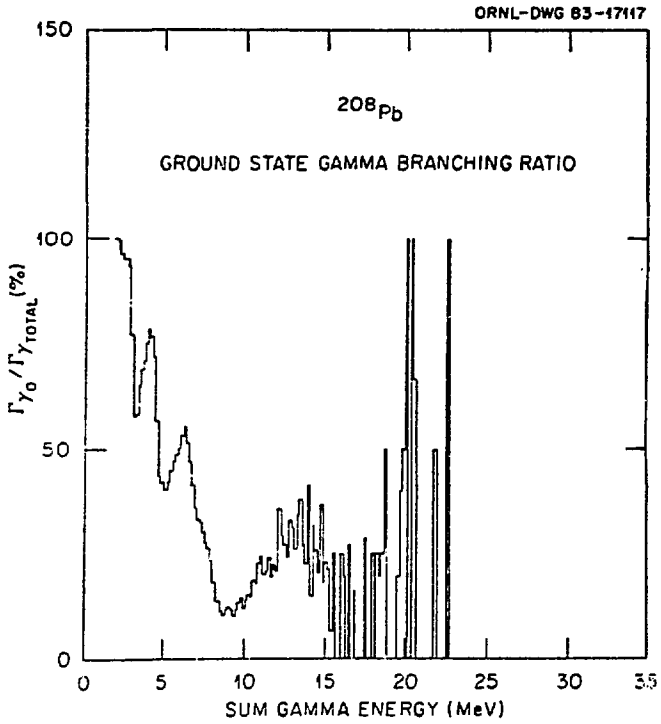


Fig. 14. Ground state gamma-ray branching ratio (%) as a function of sum gamma-ray energy (or excitation energy in $^{208}Pb$).

ground state, i.e. very collective states. In the high excitation energy region such states are defined as giant resonances. The spectrum shows the 2.61 MeV, $3^-$, state which has a branching to the ground state of 100%. The peak at ~ 4 MeV arises from excitation of the $2^+$ and $4^+$ states in $^{208}Pb$. It is not completely clear what provides the strong ground state enhancements in the 6 MeV region other than a group of $1^-$ states in that energy region. The ground state branching ratio then falls rapidly at the neutron separation energy but begins to rise again near 10 MeV. An obvious broad structure is observed in the 10-17 MeV energy region. Two peaks are found in this region, one at ~ 11 MeV, the other at ~ 13.5 MeV. These energies correspond with the known energies of the giant quadrupole and giant dipole resonances, respectively. It is to be noted that any L=4 or 6 strength in the GQR region would not have an observable ground state decay. Furthermore, the giant monopole resonance would not have a ground state gamma branch. Thus, the peaks at 11 and 13.5 MeV are from "clean" excitations of the GQR and GDR. It would of course be of great interest to have the angular distributions of the γ-rays in the

10-17 MeV region so one could sort the E1 and E2 transitions. Such information is contained in the data but is not yet analyzed.

From the spectrum in figure 14 it is possible to calculate the GQR ground-state decay width and thus, a model-independent B(E2). (These values are preliminary.) At present we must estimate the E1 tail underlying the E2 peak; angular distributions will ultimately allow a precise E2 determination. We have also corrected the data for the underlying continuum. The continuum as defined by the solid curve drawn in figure 4 is only 25-30% of the total cross section in the GQR region. We believe the continuum is likely to have only a very small ground-state $\gamma$-ray branch. The uncertainties we show include contributions from the background estimate and E1 tail.

From the ratio of the total inelastic spectrum to the inelastic spectrum in coincidence with the GQR $\gamma$-ground state branch we obtain:

$$\frac{\Gamma\gamma_{g.s.}}{\Gamma_{Total}} = (1.1 \pm 0.2) \times 10^{-4}$$

We assume the spreading width of the GQR in $^{208}Pb$ is equal to the GQR experimentally observed width ($\Gamma_{Total}$) which we take as 2.4 ± 0.2 MeV.

$$\Gamma\gamma_{g.s.} = (2.5 \pm 0.5) \times 10^2 \text{ eV},$$

$$B(E2)\uparrow = \frac{\Gamma\gamma_{g.s.} \times 2.087 \times 10^7}{E^5\gamma \, A^{4/3}} = 0.1103 \times \Gamma\gamma_{g.s.},$$

$$B(E2)\uparrow = 21 \pm 4 \text{ Wu},$$

after correction for E1 tail and underlying continuum.

For 100% EWSR,

$$B(E2)\uparrow = 26 \text{ Wu},$$

thus we find that the GQR in $^{208}Pb$ depletes 81 ± 15% of the EWSR.

This value is in excellent agreement with values deduced[1] from inelastic hadron scattering. The data also yield a value of 30% ± 6% for the GQR ground state branch.

Using a technique similar to that used to isolate single γ-ray events to the ground state, cascade events proceeding in two steps to the ground state can be studied. The gamma energy resolution is adequate to allow, for most low-lying states in $^{208}$Pb, a gate to be set on at least one γ-ray deexciting each level. In this manner, the yield of two-step γ-cascades from the continuum region through different spin low-lying states may be directly deduced. Using the technique we find the following branching for the GQR region through low-spin states:

| | | |
|---|---|---|
| g.s. | $0^+$ | 20% |
| 2.614 | $3^-$ | $\lesssim$ 2% |
| 4.085 | $2^+$ | 3-4% |
| 4.845 | $1^-$ | 2-3% |
| 4.974 | $3^-$ | 50% |
| ~ 5.5 (group) | | ~ 6% |
| 6.315 | $1^-$ | 5% |

The most striking feature of this decay scheme is the lack of GQR decay to the very collective $3^-$ state at 2.614 MeV. Rather, the GQR decays primarily through the 4.974-MeV, $3^-$, state. These results clearly demonstrate the power of the γ-decay measurement to provide microscopic nuclear structure information about high-lying giant resonances.

We also observe gamma-ray decay from the GQR excitation energy region to high spin ($4^-$, $5^-$) low-lying states. These decay branches and the percent feeding are shown on figure 15. It is clear that these decay branches cannot be from the GQR ($2^+$), but must be from $4^+$, $5^-$, or $6^+$ levels in the GQR region. Since it is unlikely from theoretical considerations that $5^-$ strength is located at $2\hbar\omega$, our gamma decay scheme clearly indicates the presence of $4^+$ and/or $6^+$ strength in the GQR region. This result is in agreement with the recent observation[4] of L=4 strength in $^{208}$Pb at 12.0 MeV using the (p,p') reaction. No decay to high spin states was observed for $^{208}$Pb excitation energies above ~ 13.5 MeV.

The gamma decay from the region of the giant dipole resonance (GDR) and giant monopole resonance (GMR) is shown on figure 16. One

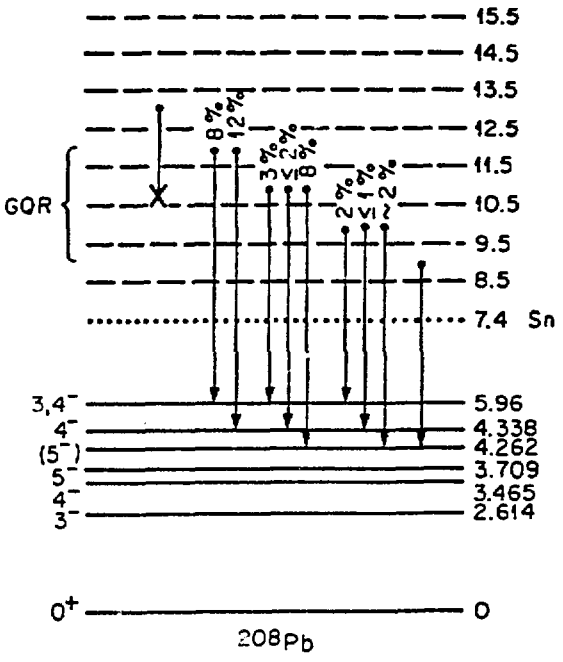


**Fig. 15.** Gamma-ray decay from 1-MeV bins of the excitation energy region of the giant quadrupole resonance to high spin states in $^{208}Pb$. The "X" indicates that no decay to high spin states was seen for energy regions above ~ 13.5 MeV of excitation energy in $^{208}Pb$.



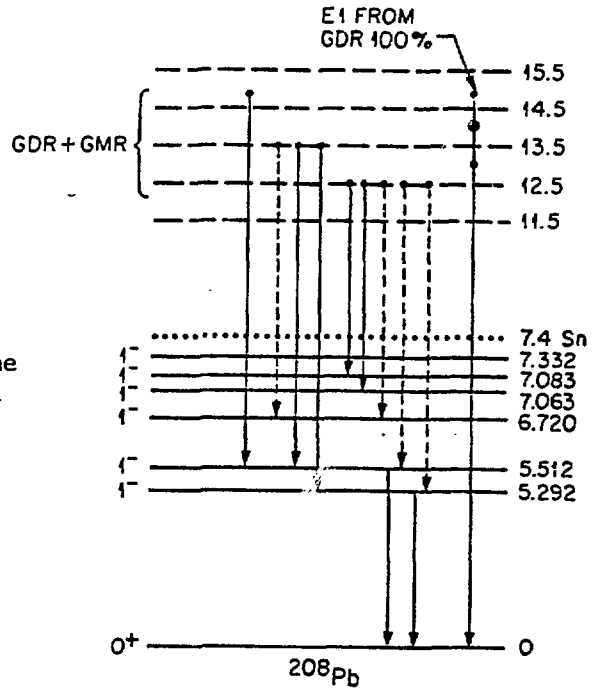


**Fig. 16.** Gamma-ray decay scheme in the excitation energy region of the giant dipole and giant monopole resonances in $^{208}Pb$.

would expect the gamma decay of the GDR to consist of an essentially 100% branch to the ground state since this strongly enhanced E1 transition should be orders of magnitude stronger than any conceivable competing gamma transition. The peak at ~ 14 MeV in figure 14 arises from gammas to the ground state from the GDR. Of course, this clearly shows that the GDR is excited by the $^{17}O$ probe. It is possible to use these GDR $\gamma$-rays to check the calculation of the Coulomb excitation of the GDR. At 13.5 degrees the GDR is calculated to have a cross section of ~ 3 mb/sr (~ 5% of the total counts in the singles spectrum at 13.6 MeV of excitation energy). If we assume that the GDR exhausts 100% of the T=1, L=1 EWSR then the expected number of GDR gammas is consistent with what we observe.

In addition to the GDR ground state gammas the only other gamma-ray transitions observed from the GDR-GMR region are those to low-lying $1^-$ states shown on figure 16. These transitions are certainly from the GMR and provide a unique signature for the GMR.

In summary, we have measured the photon decay from the giant resonance region of $^{208}Pb$. The major results are:

1) The branching for $\gamma_{g.s.}$ from the GQR yields a preliminary value:

$$B(E2)\uparrow = 21 \pm 4 \text{ Wu } (81\% \pm 15\% \text{ EWSR})$$

2) The largest GQR $\gamma$-branch is ~ 50% to the 4.974 MeV, $3^-$, state.

3) Very little GQR decay is observed to the very collective 2.61-MeV, $3^-$, state.

4) The $\gamma$-decay in the GQR excitation energy region clearly shows feeding to high spin states, indicating the presence of L=4 or L=6 strength in the GQR region.

5) The $\gamma$-decay results show that both the GMR and GDR are excited in the heavy-ion inelastic scattering reaction.

## REFERENCES


1) Fred E. Bertrand, Annual Review of Nuclear Science 26, 457 (1976). "Giant Multipole Resonances," Proceedings of the Giant Multipole Resonance Topical Conference, Oak Ridge, Tennessee, October 1979, ed. Fred E. Bertrand (Harwood Academic Publishers, New York, 1980). Fred E. Bertrand, Nucl. Phys. A354, 129c (1981).

2) T. P. Sjoreen, F. E. Bertrand, R. L. Auble, E. E. Gross, D. J. Horen, D. Shapira and B. Wright, Phys. Rev. C 29, 1370 (1984).

3) F. E. Bertrand, G. R. Satchler, D. J. Horen, J. R. Wu, A. D. Bacher, G. T. Emery, W. P. Jones, D. W. Miller and A. van der Woude, Phys. Rev. C 22, 1832 (1980).

4) J. R. Tinsley, D. K. McDaniels, J. Lisantti, L. W. Swenson, R. Liljestrand, D. M. Drake, F. E. Bertrand, E. E. Gross, D. J. Horen and T. P. Sjoreen, Phys. Rev. C 28, 1417 (1983).

5) M. Jääskeläinen, D. G. Sarantites, R. Woodward, F. A. Dilmanian, J. T. Hood, R. Jääskeläinen, D. C. Hensley, M. L. Halbert and J. H. Barker, Nucl. Instrum. Methods 204, 385 (1983).

6) F. Bortignon and R. A. Broglia, Nucl. Phys. A317, 405 (1981). G. E. Bertsch, P. F. Bortignon and R. A. Broglia, Rev. Mod. Phys. 55, 287 (1983).

## DISCLAIMER

This report was prepared as an account of work sponsored by an agency of the United States Government. Neither the United States Government nor any agency thereof, nor any of their employees, makes any warranty, express or implied, or assumes any legal liability or responsibility for the accuracy, completeness, or usefulness of any information, apparatus, product, or process disclosed, or represents that its use would not infringe privately owned rights. Reference herein to any specific commercial product, process, or service by trade name, trademark, manufacturer, or otherwise does not necessarily constitute or imply its endorsement, recommendation, or favoring by the United States Government or any agency thereof. The views and opinions of authors expressed herein do not necessarily state or reflect those of the United States Government or any agency thereof.